PNAS
www.pnas.org

Supplementary Information for

Inactivation of common microbial allergens by perfluoroalkyl chemicals modulates early-life allergic asthma

Mengjing Wang, Qianqian Li, Meifang Hou, Louisa LY Chan, Meng Liu, Soo Kai Ter, Ting Dong, Yun Xia, Sanjay H Chotirmall, and Mingliang Fang.

To whom correspondence may be addressed. Email: yunxia@ntu.edu.sg or mlfang@ntu.edu.sg.

This PDF file includes:

Materials and Methods

Reagents

We selected the top seven most abundant PFCs in the sera of children reported by previous epidemiological studies (1, 2) (table S2; Supplementary Materials, "Full names of the PFCs"), and the structures are shown in fig. S7. PFOS, PFHxS, and PFHpS (solid, purity >95%) were obtained from Dr. Ehrenstorfer (Augsburg, Germany). PFOA, PFNA, PFDA, and PFUnA (solid, purity > 95%), and the PPARα agonist ciprofibrate were purchased from Sigma–Aldrich (Singapore). The PPARα antagonist, GW6471, was purchased from Tocris Bioscience (Singapore). Stock solutions were prepared in dimethyl sulfoxide (DMSO) and stored at –40 °C. LPS and LTA were purchased from Sigma–Aldrich. LPS: *E. coli* 0111:B4, *Pseudomonas aeruginosa* 10, *Salmonella enterica* serotype Typhimurium, *Klebsiella pneumoniae*, and *Proteus vulgaris*. LTA: *Bacillus subtilis* and *Enterococcus hirae*. House dust mite (HDM) extracts were obtained from Greer Laboratories (Lenoir, NC). Ultrapure lipopolysaccharide (LPS) was purchased from Beyotime (Shanghai, China). Mouse monoclonal antibodies for flow cytometry were as follows: CD11c (clone N418, eBioscience), I-A/I-E (Clone M5/114.15.2, Biolegend), CD11b (clone M1/70, Biolegend), CD103 (clone M290, Biolegend), and CD64 (clone X54-5/7.1, Biolegend). Primary antibodies against phosphorylated-p65 (Ser536) (93H1), and NF-*κ*B p65 (D14E12) were purchased from Cell Signaling Technology. All solvents were HPLC-grade and were obtained from Fisher Chemicals (Fair Lawn, NJ).

LAL assay

LPS bioactivity were measured using the LAL assay. The samples were kept on ice, diluted in pyrogen-free water plus 0.05% Tween 20, centrifuged at 2,500 *g* for 10 min, and stored frozen at –20 °C. The LAL assay (Zhanjiang A&C Biological Ltd., Guangdong, China) was performed according to the manufacturer's instructions. In this assay, the LPS-activated protease cleaves the substrate to generate the chromogenic product p-nitroaniline.

Molecular dynamic simulation of the interactions between PFOS with LPS and LTA

CHARMM-GUI was used to generate the three-dimensional (3D) structures and topology files of LPS, PFC, and LTA (3, 4), which are presented using CHARMM36 force field files (5). We performed energy minimization to reach the maximum force <1000 kJ/mol. Equilibrating the system was performed under a 100 ps NVT ensemble, followed by 100 ps NPT ensembles at 298 K. Molecular dynamic data were collected for 100 ns in the NPT ensemble at 298 K, and GROMACS 5.1.4 software was used to constrain hydrogen bonds, allowing for an integration interval of 2 fs. A cutoff = 1.0 nm was used for long-range van der Waals energies, and the particle mesh Ewald method (6) was used for computing electrostatic interactions. The nonbonded pair lists were updated every 0.010 ps. The coordinates were saved every 100 ps. Images were generated using YASARA (version 16.7.22).

QSAR model

A quantitative structure-activity relationship (QSAR) model was developed to analyze the chemical inactivation potencies associated with their structural and chemical characteristics. The model was built upon a theoretical molecular descriptor calculation, and the molecular descriptors were calculated using the PaDel descriptor, which is open-source software dedicated to providing molecular descriptors calculations (7). This software allows users to retrieve 1,875 descriptors based on the input of molecular information in the sdf format. We calculated 1445 1D and 2D molecular descriptors for each molecule. Many molecular descriptors highly correlated, constant, or nonvalues. Therefore, reduction of the sizes of descriptors was manually performed in R (19). Molecular descriptors that are highly correlated (Pearson correlation no less than 0.9), nonvalues, and constant were removed, resulting in 489 molecular descriptors that were retained for each test chemical, which may lead to over-fitting problems. Associations among the resulting molecular descriptors of the test PFCs with their $EC_{20/30}$ values were determined using Pearson correlation analysis.

Transmission electron microscopy (TEM) of LPS

To determine the effect of the test PFCs on the native structure of LPS, LPS from *E. coli* 0111:B4 (5.0 mg/mL in 0.1 M Tris-HCl, pH 7.2) was incubated with 1 mM of each PFC for 6 h at 25 °C, and samples (4 μL) were placed on glow-discharged 12-nm carbon-coated copper grids and stained with 1% (v/v) uranyl acetate (Sigma–Aldrich, Singapore) for 1 min. Electron micrographs were recorded using an Tecnai Spirit

T12 transmission electron microscope (FEI Company) equipped with a 4k × 4k-pixel Eagle CCD camera operated 120 kV.

In vitro gut reactor system set-up

A compact chemostat system with controlled temperature, dissolved oxygen (DO), flow rate and pH has been set-up as shown in fig. S10. The working volume was maintained at 2 L with residence time of 2.8 days. The temperature was monitored at 37°C. Before inoculation, the whole reactor chamber with medium was autoclaved for sterilization. Then the outlet for gas collection was open and the medium inside was flushed with N_2 through the N_2 purge inlet connected with a 0.22 µm gas filter for at least an hour. The fresh fecal sample from one healthy donor was transferred to anaerobic chamber within 1 h. Approximately 20 g sample was mixed with growth media and settled for 5 min to remove large particles. Then the supernatant was transferred to the pre-reduced reactor medium for inoculation. The N_2 purging continued for several hours after inoculation. Then the N_2 purge inlet was closed, and the gas collection outlet was connected with an empty gas bag to collect any gas production. To maintain the anaerobic condition of the influent, the medium bottle was immediately connected with a gas bag filled with N_2 gas after being autoclaved while the medium inside was still hot. Effluent bottle was also autoclaved and flushed with N_2 through a filtered inlet. After N_2 flushing, another empty gas bag was then connected to avoid oxygen leakage to the system. The gut reactor was sampled three times a week for routine monitoring of OD_{600}, chemical oxygen demand (COD), and short-chain fatty acid (SCFA) measurement.

To investigate whether the total LPS can be inactivated by PFOS, the filtrates were prepared by filtering incubated bacterial cultures using 0.2 µm Acrodisc syringe filter (Gelman Laboratory, MI), and then incubated with tested chemicals for 6 hours at 25 °C as mentioned above. Total LPS only was used as a positive control.

Molecular docking analysis of the interactions of PFOS with Der p1

We used AutoDock 4.2 (La Jolla, California, USA) to determine the binding modes of PFOS to Der p1 (PDB, 1XKG). Autodock 4.2 (8) with a Lamarckian genetic algorithm (9) was employed for selecting the docking mode selection because of its high reproducibility (10, 11). AutoDockTools 1.5.6 (12) was used to determine protein charge, and the data were saved as a PDBQT file. The 3D structure of PFOS was generated using ChemDraw ultra 2.0 (13), and VEGA ZZ 3.1.2 (14) was used to calculate and add the MOPAC charge to the ligand. Avogadro 1.2.0 (15) was utilized to optimize the structure of 1β-hydroxy alantolactone using the method of steepest descent and gradient descent. AutoDock Tools 1.5.6 was used to prepare a PDBQT file for input into the subsequent docking program. The docking calculations were performed by locating a 50 × 50 × 50 grid-point map with 0.375 Å grid-point spacing, which encompassed the catalytic sites. Each ligand was docked 100 times to retrieve the optimum docking conformations.

Molecular dynamic simulation of the interactions of PFOS with Der p1

The conformations of Der p1 bound to PFOS were further optimized using molecular dynamic simulation, which was performed using GROMACS 5.1.4 (16). Amber99sb Force Field and the tip3p water condition were selected during the topology process. Two types of systems were placed in the box at least 1.0 nm from the box edge. We performed energy minimization to reach a maximum force <1000 kJ/mol. Equilibrating the water around the protein was performed under 100 ps NVT followed by 100 ps NPT ensembles at 298 K. Molecular dynamic data were collected for 100 ns in the NPT ensemble at 298 K, and GROMACS 5.1.4 was used to constrain hydrogen bonds, allowing for an integration interval of 2 fs. A cut-off = 1.0 nm was used for long-range van der Waals energies, and the particle mesh Ewald method (6) was used to compute electrostatic interactions. The nonbonded pair lists were updated every 0.010 ps. The coordinates were saved every 100 ps.

Analysis of bronchoalveolar lavage fluid (BALF)

Mice were anesthetized and exsanguinated by cutting the inferior vena cava. Bronchoalveolar lavage was performed three times using 1 ml of PBS containing 5 mM EDTA. The recovered BALFs were combined and centrifuged at 700 g for 5 min at 4 °C. The cell pellets were resuspended in PBS, and total cell numbers were counted using a Cellometer (Nexcelom). Eosinophils, neutrophils, and lymphocytes were enumerated after staining with Wright-Giemsa staining.

Measurement of airway responsiveness (AHR)

In the HDM-induced allergic asthma model, mice were anesthetized, the trachea was intubated, and the lungs were mechanically ventilated. Lung resistance (RL) was measured after increasing doses (10–100 mg/ml) of aerosolized methacholine (Sigma) was applied (Buxco Electronics).

Flow cytometry

To measure immune cell subsets, lungs were perfused and then instilled with 1 ml of digestion buffer (RPMI 1640 containing 1 mg/ml collagenase IV and 5 U/ml DNase I; Sigma–Aldrich). Excised lungs were cut into small pieces, incubated in 2 ml of digestion buffer at 37 °C with shaking at 220 rpm for 1 h, filtered through a 70-mm cell strainer, and the red blood cells were lysed using RBC lysis buffer (eBioscience). Cells were collected by centrifugation and counted. For flow cytometric analysis, cells were incubated with an Fc-blocking antibody (purified anti-mouse CD16/32, BioLegend) to prevent binding of nonspecific FcγRIII/II and then incubated with fluorochrome-conjugated antibodies for 1 h on ice. After washing, the samples were analyzed using a BD LSRII Flow Cytometer, and data were processed using FlowJo software (TreeStar).

Analysis of immunoglobulin levels

The serum levels of total IgE, HDM-specific IgE, IgG1, and IgG2a were measured using ELISA kits purchase from Wuhan Biotech Co, Ltd, China according to a standard published protocol (17).

Histology

Left Lungs were excised, fixed in 4% paraformaldehyde, and sections were prepared and stained with H&E or periodic acid-Schiff (PAS). The samples were examined using a Nikon E200 microscope to identify inflammatory cell infiltration, tissue damage, and mucus production. For each mouse, five random fields of view were digitized (these images included both bronchioles and blood vessels) using a microscope. The histopathology scoring values of lung injury followed one previous study conducted by Sharma et al. (2011) (18). The histopathological changes were scored in a blind manner and graded on a subjective scale of 0-4, corresponding to mild, moderate, marked, or severe inflammation; respectively, with an increment of 0.5 if the inflammation fell between two integers. The mean score was then calculated for each individual mouse. The final values are expressed as a box and whisker plot for each group of mice.

Cytokine production

Single-cell suspensions were obtained by homogenizing mediastinal lymph nodes through a 100-μm cell sieve. Cells were treated ex vivo with 15 μg/ml HDM for 3 days, and supernatants were analyzed using ELISA kits to detect IL-5, IL-13, IL-17A, IL-10, and IFN-γ (Shanghai MLBIO Biotechnology Co. Ltd).

Transcriptomic Analysis

Total RNAs extracted from mouse lung tissues and HNECs using Trizol reagent (Tiangen Biotech Co., Ltd., Beijing, China) were sent to Novogene Ltd., Beijing, China for library preparation and next-generation sequencing. mRNA was purified using poly-T oligo-attached magnetic beads and randomly fragmented in fragmentation buffer for library construction. Sequencing libraries were generated using an NEBNext Ultra RNA Library Prep Kit for Illumina (New England Biolabs, Ipswich, MA, USA). The library preparations were sequenced using an Illumina HiSeq 4000 platform to generate 150-bp paired-end reads. The sequenced reads/raw reads containing low-quality reads or reads containing an adaptor were filtered to obtain clean reads, and these clean reads were subsequently mapped to a reference genome using HISAT (version 2.0.5). To analyze gene expression levels, fragments per kilobase of transcript per million mapped reads were calculated using HTSeq (version 0.6.1). Differential gene expression analysis (six experiments) was performed using DESeq2 (version 1.10.1, Bioconductor), and differences in gene expression ($P < 0.05$) were defined as differentially expressed. Cluster analysis of the DEGs was applied to determine expression patterns. Gene Ontology (GO) enrichment analysis of the DEGs was performed using GOseq R packages. KOBAS was used to test for significant enrichment of DEGs in KEGG pathways. Gene set enrichment analysis (GSEA) was performed to analyze the enrichment pathways generated from the two DEG sets described above, with a cutoff of FDR < 0.25 and $P < 0.05$.

To determine the relationship between transcript levels and treatment group (control vs treatment), we used WGCNA in the R package (19). Briefly, the expression correlation coefficients were calculated to select a suitable soft threshold to build gene networks using a scale-free topology model. Subsequently, gene expression modules with similar patterns were identified according to a gene cluster dendrogram

using the dynamic tree cut method (minModuleSize = 50 and mergeCutHeight = 0.25). To identify modules that were significantly associated with the traits of samples, the module eigengenes were calculated and correlated with the groups. Modules with high correlation values ($P < 0.05$) were considered significant trait-related modules. The correlated genes ($P < 0.05$), were considered putatively related to the group.

Validation of transcriptome analysis using quantitative real time PCR (RT-PCR)

RNA from lungs was purified using an RNA isolation kit (Tiangen) and then reversely transcribed (Tiangen). cDNA was analyzed by qPCR using SYBR green reagents (Thermo) with the ABI 7300 system. The primers used for RT-PCR were listed in table S1. GAPDH was used as the reference gene to normalize the gene expression data.

Cell culture and treatments.

The THP-1 cell line (ATCC TIB-202) was cultured in RPMI 1640 supplemented with 10% FBS and 2 mM L-glutamine in a humidified atmosphere containing 5% CO_2 at 37 °C. Monocyte-like THP-1 cells were differentiated in a medium containing 100 ng/mL phorbol 12-myristate 13-acetate for 48 h. After maturation, THP-1 macrophages were cultured in the normal medium.

The human pulmonary epithelial cell line A549 were grown in Ham's F-12K (Kaighn's) Medium (Gibco) with 10% (v/v) heat-inactivated fetal calf serum (Gibco), 100 U/ml penicillin, and 100 µg/ml streptomycin in 75-cm^2 culture flasks at 37 °C in a humidified atmosphere with 5% CO_2. A flask containing 70–80 % confluent cells was subcultured in a 96-well plate (50,000 cells/well) and cultured with serum-free medium for 24 h.

Flocked nasopharyngeal swabs (FNPS) were collected from healthy volunteers (n=3, 26/F, 24/M and 34/M) with written consent (NTU Singapore: IRB-2020-05-004). HNECs were released from the swab by flushing with transport medium at least 20 times and cultured in a 1:1 ratio of advanced DMEM/F12 (Gibco, Thermofisher) and BEPICM culture medium (ScienCell), supplemented with BEpiCGS, Penicillin/Streptomycin (100 µg/ml), Primocin (50 µg/ml) (Invivogen), Y-27632 (5 µM) (Tocris), DMH-1 (1 µM) (Tocris), A83-01 (1 µM) (Tocris) , DAPT (5 µM) (Stemcell Technologies), Fibroblast growth factor 7 (25 ng/ml) (Peprotech), Fibroblast growth factor 10 (100 ng/ml) (Peprotech) and Insulin-like growth factor-1 (25 ng/ml) (Peprotech), on a human collagen IV (Sigma) pre-coated culture plate to grow as a monolayer. Media was refreshed every two days until confluence. Once confluency was reached, 2 x 105 cells were seeded at the apical chamber of a 24-well transwell (Corning transwell 3470) pre-coated with human collagen I. HNECs were then first cultured in submerged phase on transwells until intact. Media in the apical chamber was then removed and grown at air-liquid interface (ALI). Media was refreshed twice weekly and cells differentiated for at least 21 days using advanced DMEM/F12 medium (Gibco, Thermofisher) supplemented with hydrocortisone (0.5 µg/ml) (Sigma), 3,3',5-Triido-L'thyronine (100 nM) (Sigma), epinephrine (0.5 µg/ml) (Sigma), human EGF (0.5 ng/ml) (Thermofisher) and TTNPB (100 nM) (Sigma).

The cells were then exposed to LPS alone or a mixture of LPS and a PFC for 24 h. A culture medium or vehicle control group (0.1% DMSO in culture medium) was prepared as appropriate. LPS served as a positive control. In THP-1 and HNECs, LPS is 100 ng/mL; A549 cells, LPS is 1 ug/mL. In order to explore the role of the PPARα mechanism, THP-1 macrophages were dosed with the PPARα agonist ciprofibrate (20 µM) and antagonist GW6471 (5 µM). In ciprofibrate treatment, cells were pre-treated for one hour to activate the pathway before the addition of LPS or PFOS. The concentrations of tumor necrosis factor (TNF)-α in culture supernatants were determined using ELISA kits from Wuhan Biotech Co, Ltd. (Wuhan China) according to the manufacturer's instructions. LTA inactivation were determined based on TNF-α production in THP-1 macrophages stimulated with LTA/PFOS mixture.

Cell viability was determined using the alamarBlue assay. When the exposures were completed, 20 µL of resazurin (0.74 mg/mL in PBS) was added to the cell culture medium. Culture dishes were covered with metal foil and incubated at 37 °C in an atmosphere containing 5% CO_2 for 18 h. Cytotoxicity was measured by determining the fluorescence (570 nm and 600 nm) emitted by reduced resazurin (resorufin) using a microplate reader. Cell viability was expressed as the percentage viability compared with the control cells.

Western blot analysis.

Cells were lysed with M-PERTM Protein Extraction Reagent (Pierce, Rockford, IL) supplemented with a protease inhibitor cocktail (Calbiochem, San Diego, CA). The protein concentration of each sample was measured using the BCA assay (Pierce, Rockford, IL). Equal amounts of extracts were separated using

10% SDS-PAGE, electrophoretically transferred to a PVDF membrane, and then blotted as previously described (20). Actin was used as an internal control.

Transient transfections

The vectors used to express the PPARγ-ligand binding domain (LBD) were fused in-frame with the Gal4 DNA binding domain (pGal4-PPARα-LBD) and the reporter vector containing five copies of the Gal4 upstream activating sequences (pGal4UAS-luciferase) that drive the transcription of the luciferase reporter gene (GeneChem, Shanghai, China). THP-1 macrophages were transfected using the DEAE-dextran method (21). PPAR assays were performed by transfecting THP-1 macrophages with a mixture of DNA-dextran (750 μg/ml) with 70 ng of pGAL4UAS-luciferase and 35 ng of receptor vector (PPARα) per well. Cells (1.5×10^5 cells per well) were added to 96-well plates and then incubated for 48 h in complete medium (10% FBS supplemented RPMI 1640). Cells were treated with a mixture of each PFC and LPS for 3 h in RPMI 1640, harvested, and luciferase activity was measured using a dual-luciferase reporter assay kit (Promega).

Bacterial infection models.

All animal studies were conducted under protocols approved by the Animal Ethics Committee of the Research Center for Eco-Environmental Sciences, Chinese Academy of Sciences (AEWC-RCEES-2021001). Generally, females mount a stronger immune response than males, thus groups of 5 female BALB/c mice (6 weeks old, n=5 for each treatment) were injected intranasally with PFOS (10 and 100 μg/kg body weight per day) for one week before mice were intranasally infected with 10^7 CFU of *P. aeruginosa*. strain 8821, which was purchased from Beijing Beina Bio and used as the model bacterial infections for this study. *P. aeruginosa* were cultured in Luria-Bertani broth and harvested when the culture reached an OD at 640 nm of 2 U (early stationary phase). Bacteria were washed in PBS and density adjusted to an OD of 1 U before use. The control group of mice received intranasal doses of PBS. Another three groups were prepared alongside without any introduction of bacteria (i.e., PBS; 10 and 100 μg/kg body weight per day PFOS control).

Lung infection with *P. aeruginosa* and collection of bronchoalveolar lavage fluid (BALF), lung, and blood samples.

Mice were sacrificed 24 h after the infection. Bronchoalveolar lavage fluid (BALF) was obtained by lavaging the lung with 3 ×1 ml of PBS containing soybean trypsin inhibitor (100 μg/ml). BALF was centrifuged at 300 × g for 5 min at 4°C. The cell pellets were resuspended in PBS, and total cell numbers were counted using a Cellometer (Nexcelom). Eosinophils, neutrophils, and lymphocytes were enumerated after staining with Wright-Giemsa staining. The supernatants were used for cytokine analysis. The lung tissues were also obtained for cytokine production. Lung tissues were homogenized (maximum speed, 20 s, PowerGen 125; Fisher Scientific) in 50 mM HEPES buffer (4 μl/mg lung) containing soy-bean trypsin inhibitor (100 μg/ml). The homogenate was centrifuged at 4°C for 30 min at 18,000 × *g*. The supernatant was stored at -80°C for later cytokine analysis. Blood was collected by cardiac puncture. The blood was treated with heparin (Sigma; Cat No H3149), immediately placed on ice and centrifuged at 3,500 rpm for 25 min to obtain serum. The samples were stored in aliquots at -80 °C for later cytokine analysis. The levels of IL-1β, IL-6 and TNF-α in the BALF, lung, and blood were measured using ELISA kits purchase from Wuhan Biotech Co, Ltd, China according to a standard published protocol (17).

Der p1 binding to PFOS

Der p1 is the major immunogenic protein of the HDM extract tested here. We therefore investigated the effects of PFOS on the bioactivity of Der p1. PFOS was used to titrate pure HDM Der p1 (0.05 mg/mL) for 24 h at 25 °C at a concentration similar to that in the peripheral circulation of humans.

A Microcal ITC 200 calorimeter was used to measure the equilibrium dissociation constant (Kd) of the binding of PFOS to Der p1. Der p1 (20 μM in phosphate buffer, pH 7) was added to the sample cell, and 200 μM PFOS taken up in the syringe. The titration was followed using the default ITC procedure, and the raw data were fitted using a single-site binding model with Microcal Origin 5.0 software to calculate the association constant (K_a). The dissociation constant (K_d) = $1/K_a$.

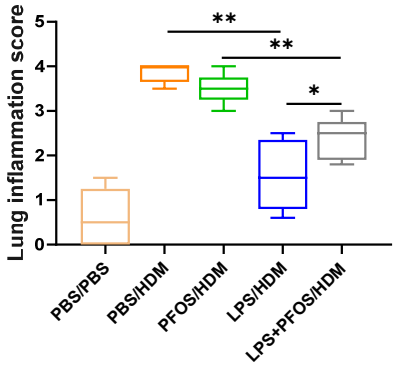

Fig. S1. Lung inflammatory scores. The values are expressed as a box and whisker plot for each group of mice (n = 5 mice per group). *$p < 0.05$, **$p < 0.01$ (ANOVA).

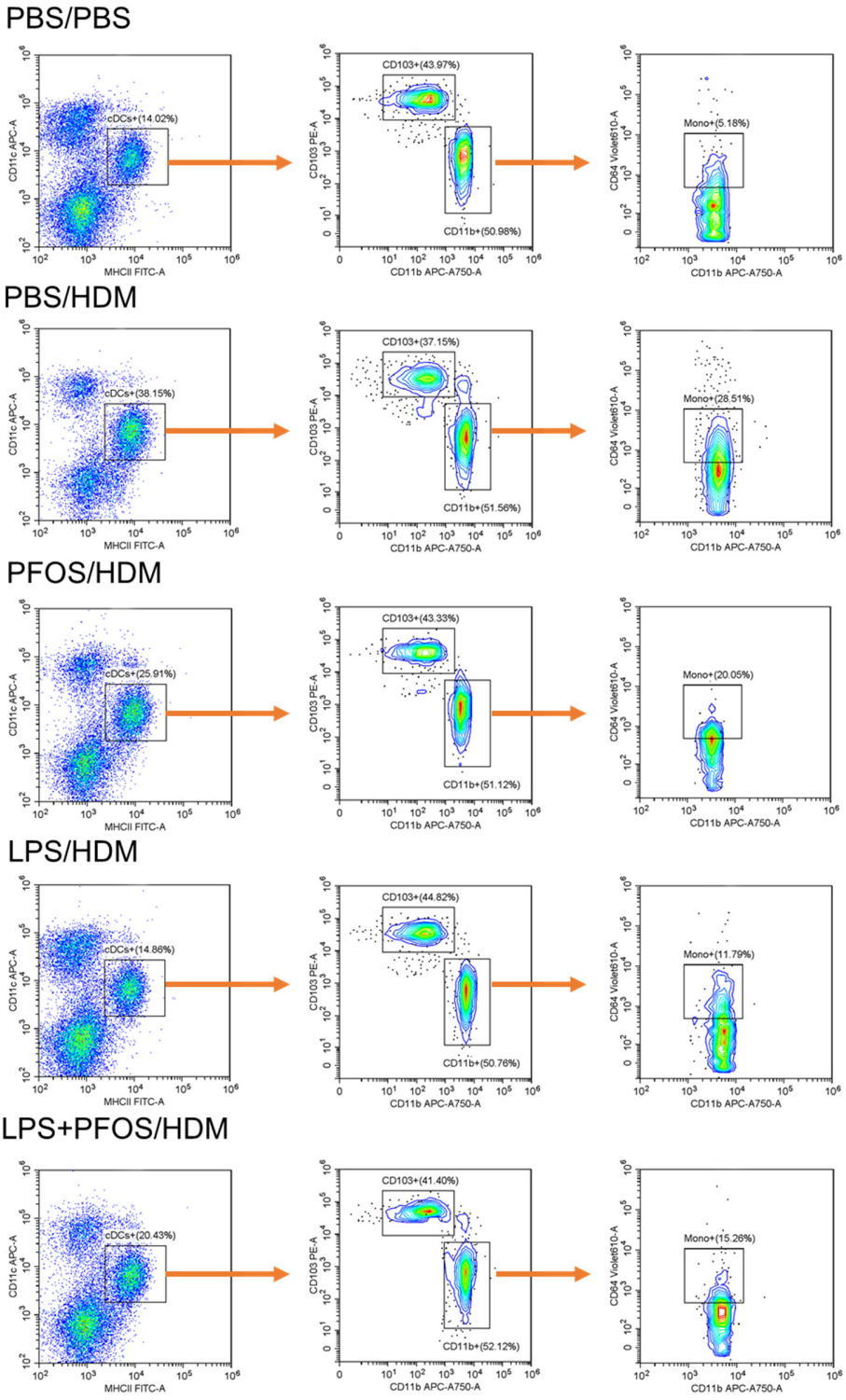

Fig. S2. Gating strategy to identify DCs and DC subsets in mouse lungs.

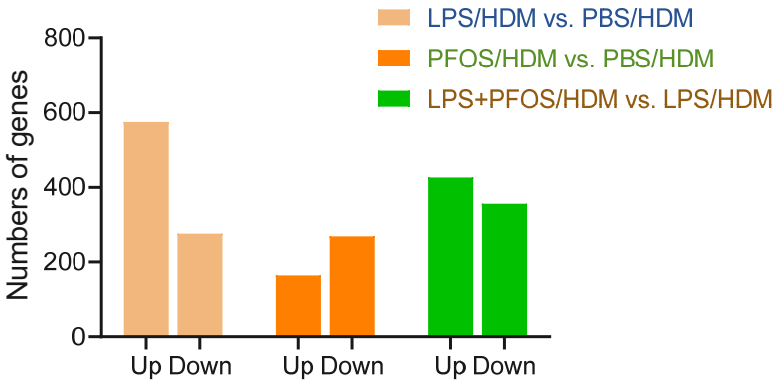

Fig. S3. Differentially expressed genes between mouse treatment groups.

A. LPS/HDM vs. PBS/HDM

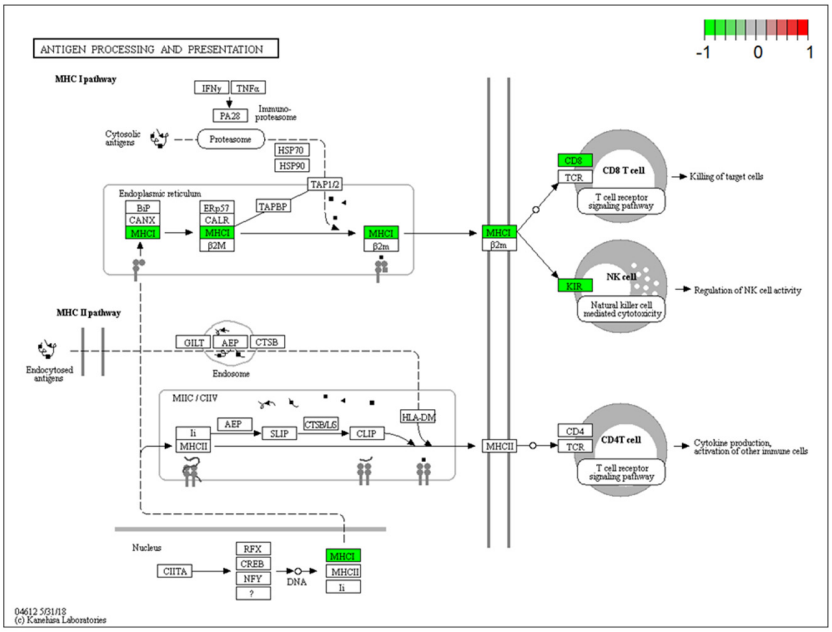

B. LPS+PFOS/HDM vs. LPS/HDM

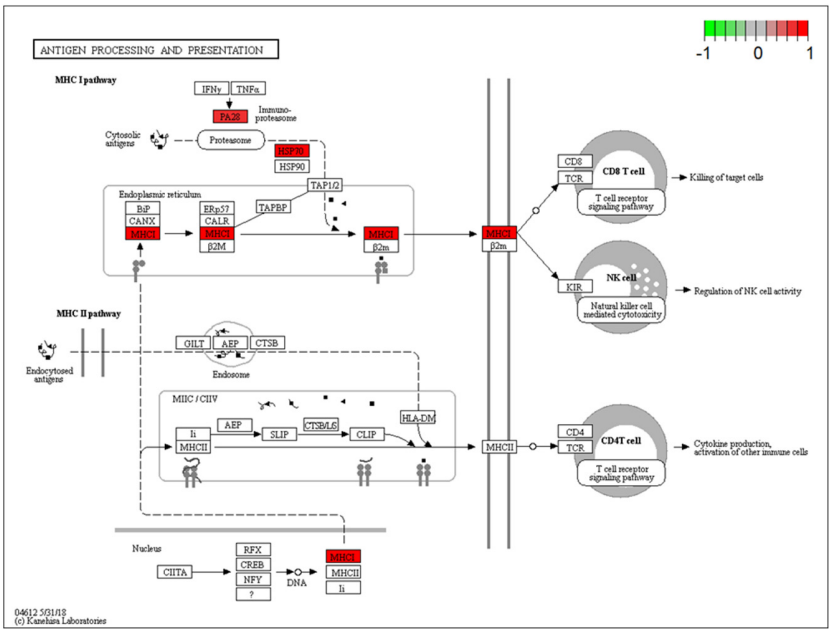

Fig. S4. KEGG pathway presentation of gene expression patterns of pathways that mediate antigen processing and presentation in response to LPS and HDM. (*A* and *B*) LPS/HDM group compared with the PBS/HDM group (*A*) and the LPS+PBS/HDM group compared with the LPS/HDM group (*B*). Red denotes significant upregulation. Green denotes significant downregulation.

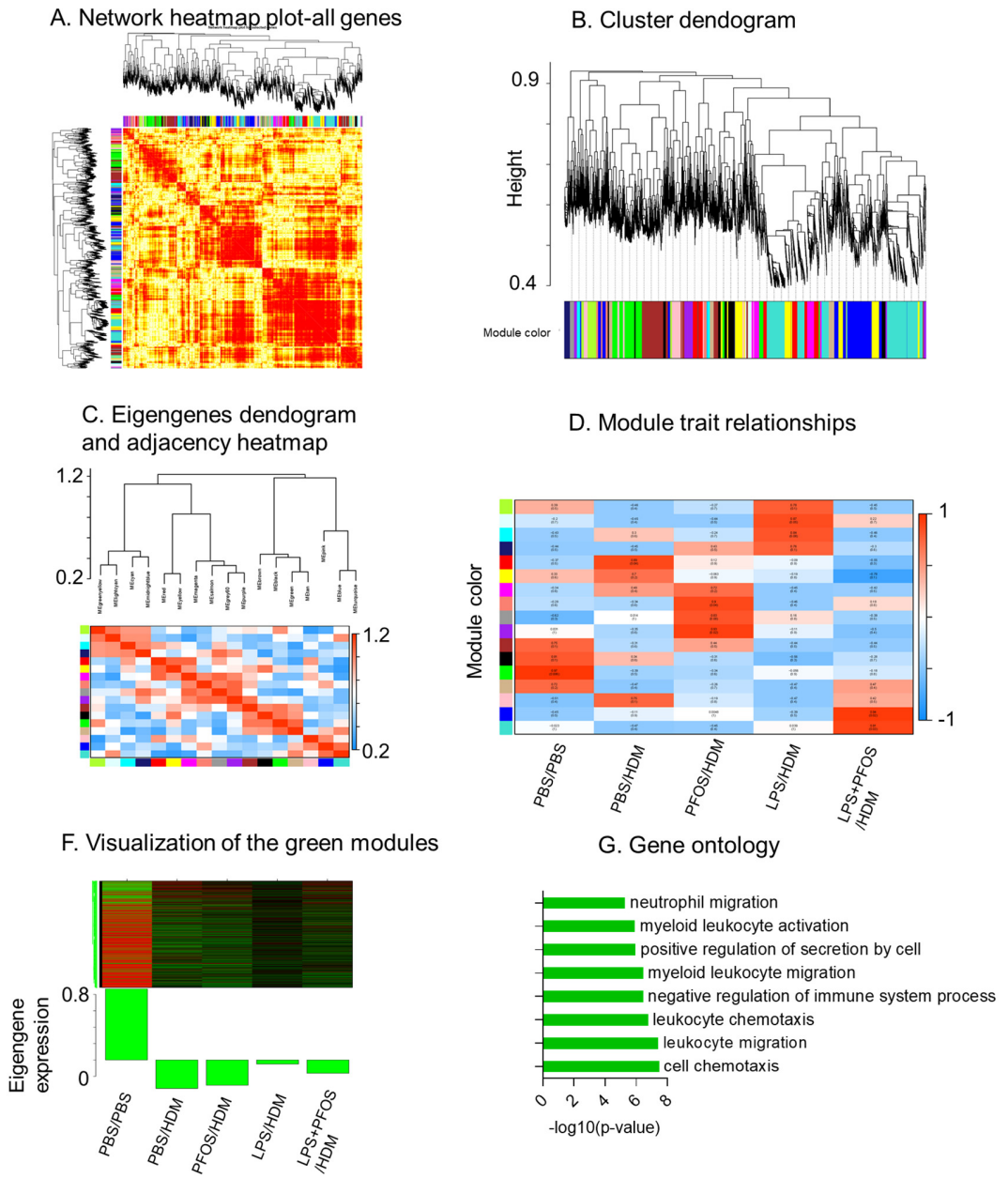

Fig. S5. Weighted Gene Coexpression Network Analysis (WGCNA). (*A*) Heatmap representing the Topological Overlap Matrix (TOM). The degree of overlap is represented by the color shade. A darker color represents higher overlap and a lighter color represents lower overlap. Gene dendrogram, left; module assignment, top. (*B*) Average linkage hierarchical clustering dendrogram. Input was the topological overlap-based dissimilarity. Modules, designated by color code, are the branches of the clustering tree. (*C*) Unsupervised hierarchical clustering heatmap and dendrogram of 16 module eigengenes. (*D*) Correlation of module eigengenes with clinical and pathological traits. Each row corresponds to a module eigengene, and the columns are clinical traits. The values in the cells are presented as “Pearson r (p value)” that are color-coded by direction and degree of the correlation (red = positive correlation; blue = negative correlation). The 16 modules of coexpressed transcripts are presented with their respective correlation parameters between clinical and pathological traits. (*F*) Visualization of the green modules. (*G*) Pathway analysis using Gene Ontology (GO) showing the top pathways enriched in the gene sets of the green modules.

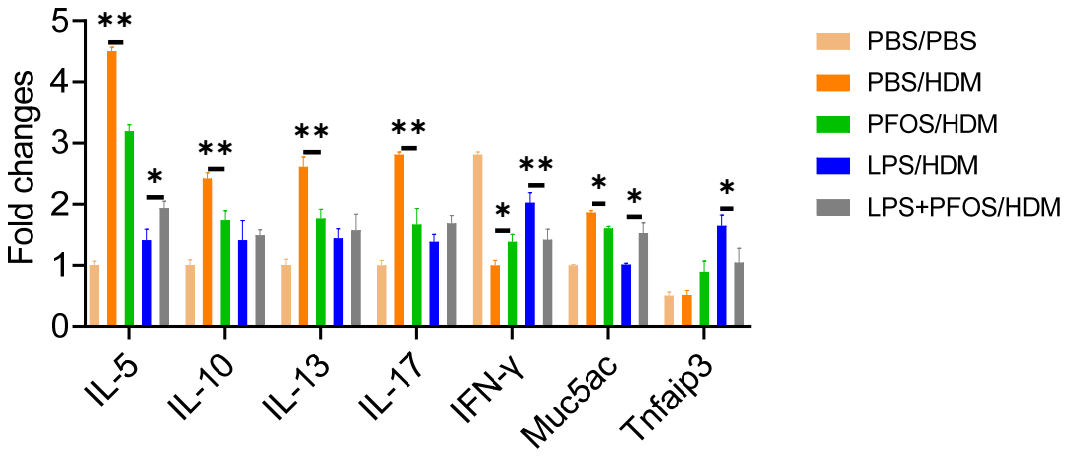

Fig. S6. RT-PCR results of 7 selected genes (IL-5, IL-10, IL-13, IL-17, IFN-γ, Muc5ac, and Tnfaip3) in mouse lung tissues from different treated groups. Data are presented as the mean ± SEM of triplicates compared with the control PBS group. *$p < 0.05$, **$p < 0.01$ (ANOVA).

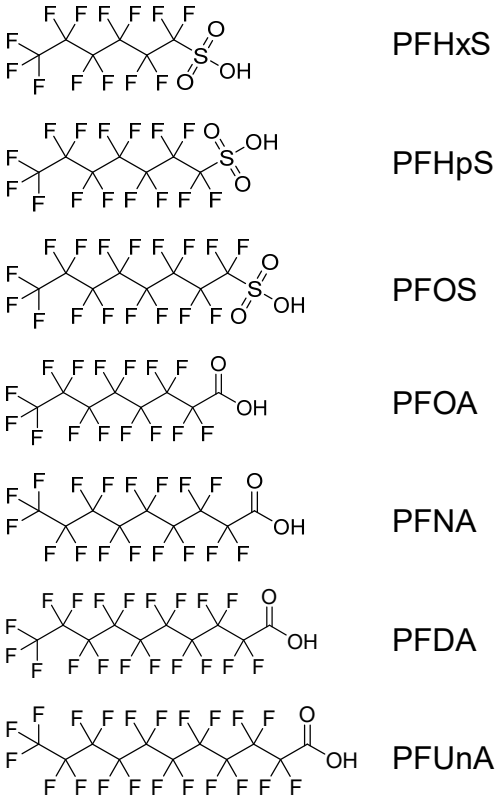

Fig. S7. Structures of the perfluorinated chemicals.

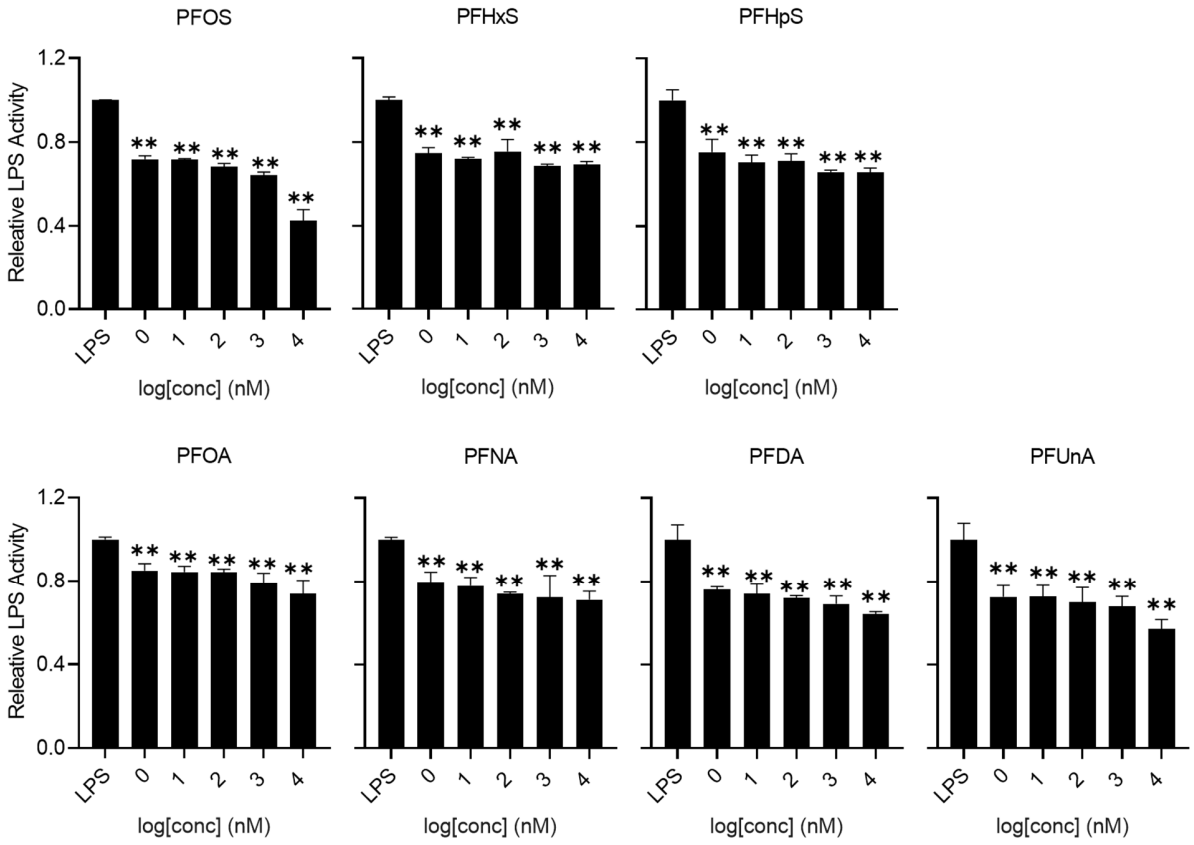

Fig. S8. PFCs inactivate the activity of purified *E. coli* LPS. Values represent mean values and the standard error of the mean relative to the LPS control (n = 3). Significant differences vs the control simultaneously treated with PFCs and purified LPS: *$p < 0.05$, **$p < 0.01$ (ANOVA).

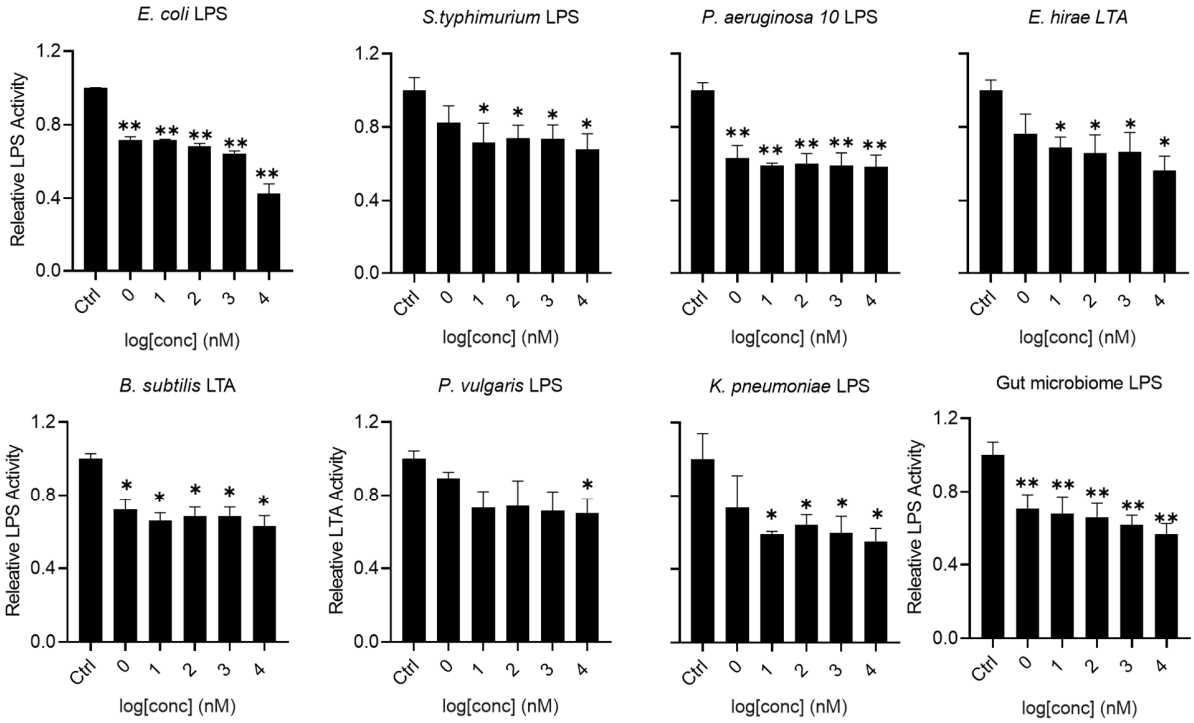

Fig. S9. Effects of PFOS on the inactivation of LPS purified from the total gut microbiome, five gram-negative bacterial species; and LTA from two gram-positive bacterial species. Values represent the mean and the standard error relative to the LPS or LTA control (n = 3). Significant differences vs the control simultaneously treated with pure LPS or LTA: *$p < 0.05$, **$p < 0.01$ (ANOVA).

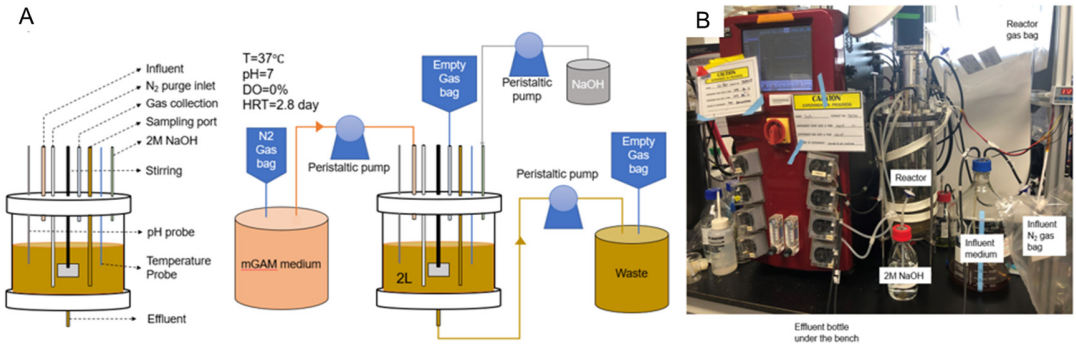

Fig. S10. In vitro gut reactor. (*A*) Diagram of the gut chemostat. (*B*) Photograph.

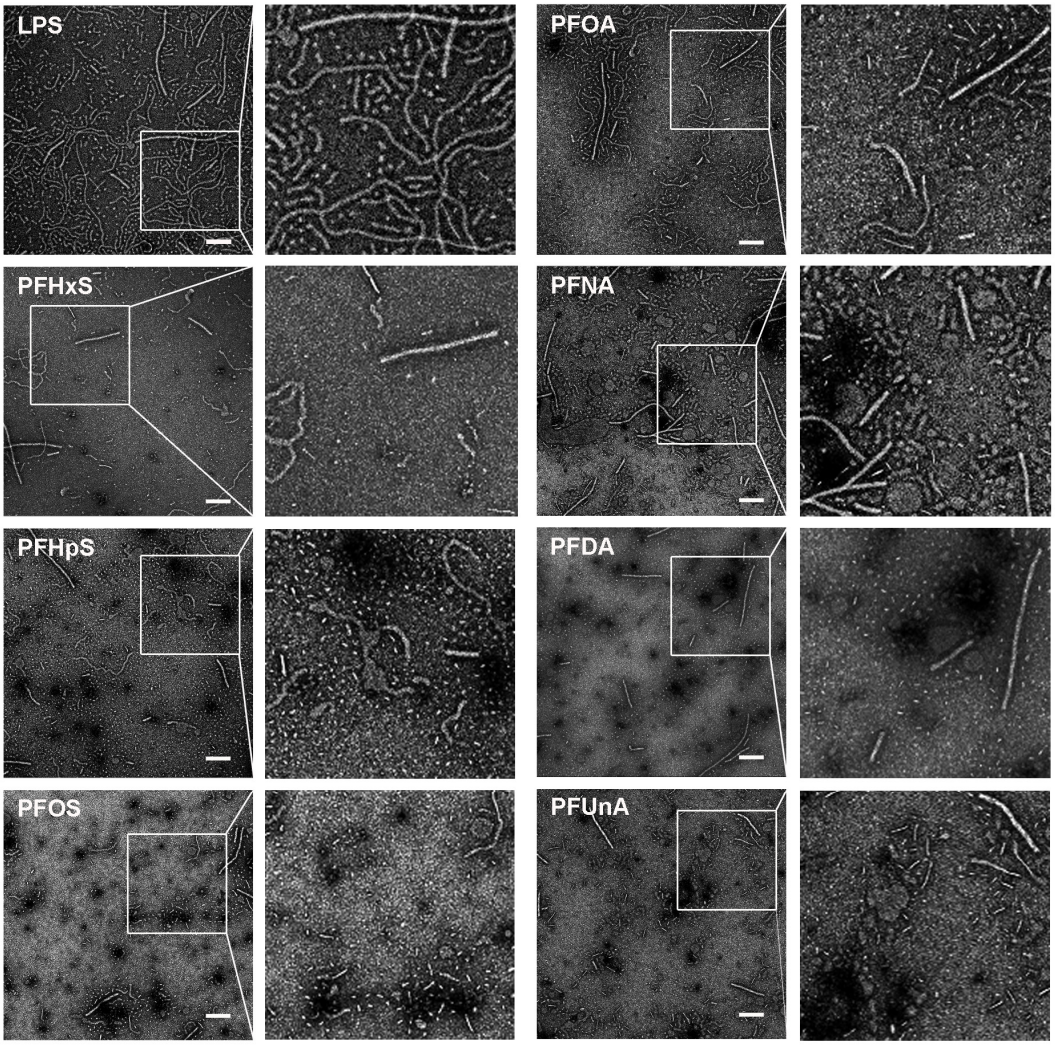

Fig. S11. PFCs disaggregate large LPS micelles to smaller LPS/PFC complexes. TEM images of *E. coli* 0111:B4 LPS. Negatively-stained samples of LPS alone, LPS after addition of PFHxS, PFHpS, PFOS, PFOA, PFNA, PFDA, and PFUnA. Scale bar = 200 nm.

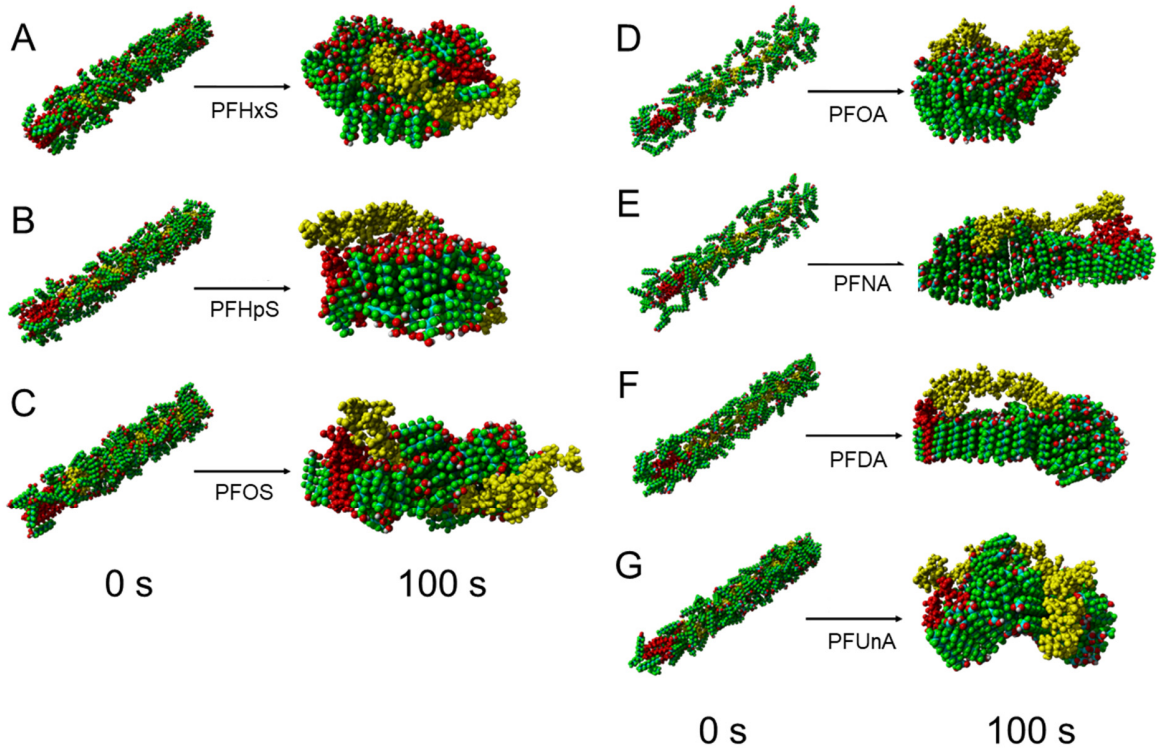

Fig. S12. Conformational changes of LPS in the presence of PFHxS (*A*), PFHpS (*B*), PFOS (*C*), PFOA (*D*), PFNA (*E*), PFDA (*F*), and PFUnA (*G*). LPS (polysaccharide, yellow; lipid A, red) and PFCs (carbon, cyan; oxygen, red; fluorine and sulfur, green).

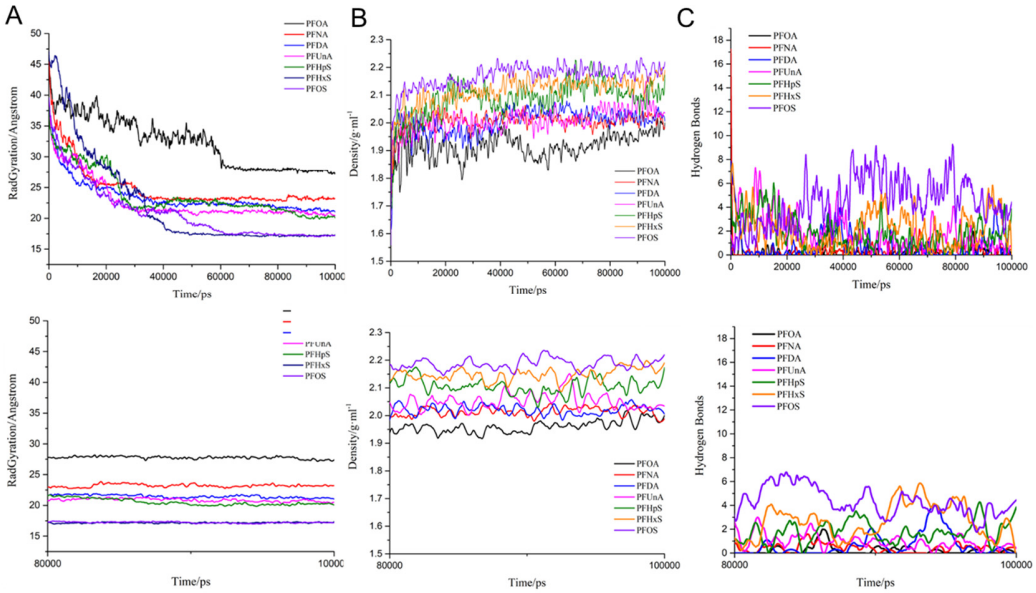

Fig. S13. Molecular dynamic simulations of PFC aggregates. (*A*) Radius of gyration (Rg) of PFC aggregates during 0–100 ns and 80–100 ns. (*B*) Density of the PFC aggregates during 0–100 ns and 80–100 ns. (*C*) Hydrogen-bond formation of PFC aggregates during 0–100 ns and 80–100 ns.

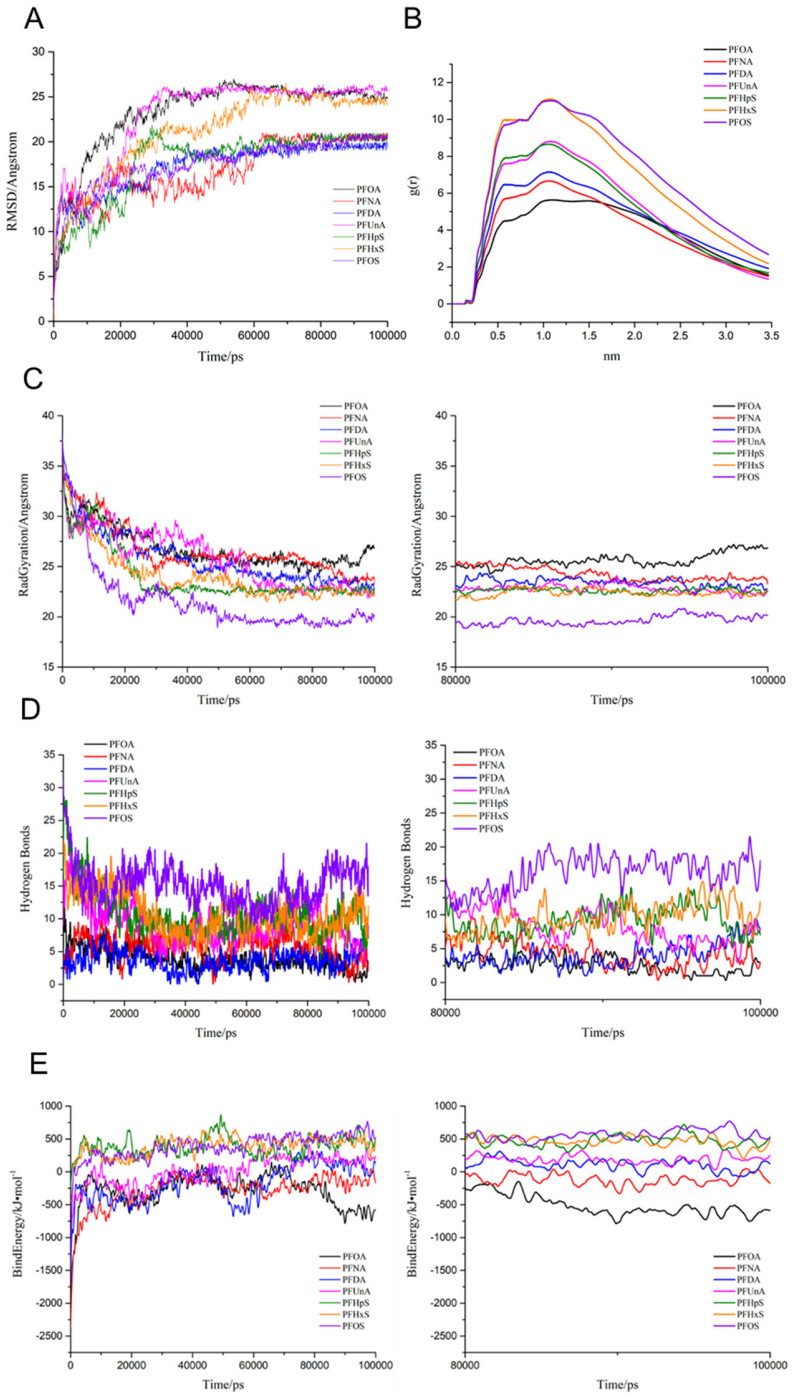

Fig. S14. Molecular dynamic simulations of LPS binding to PFCs. (*A*) Root-mean-squared deviation (RMSD) of LPS–PFC (0–100 ns). (*B*) Radial Distribution Function (RDF) of PFCs in LPS–PFC (0–100 ns). (*C*) Radius of gyration (Rg) of LPS in LPS–PFC during 0–100 ns and 80-100 ns. (*D*) Hydrogen-bond formation between LPS and PFCs during 0–100 ns and 80–100 ns. (*E*) Binding energies (kJ/mol) of LPS–PFC during 0–100 ns and 80–100 ns.

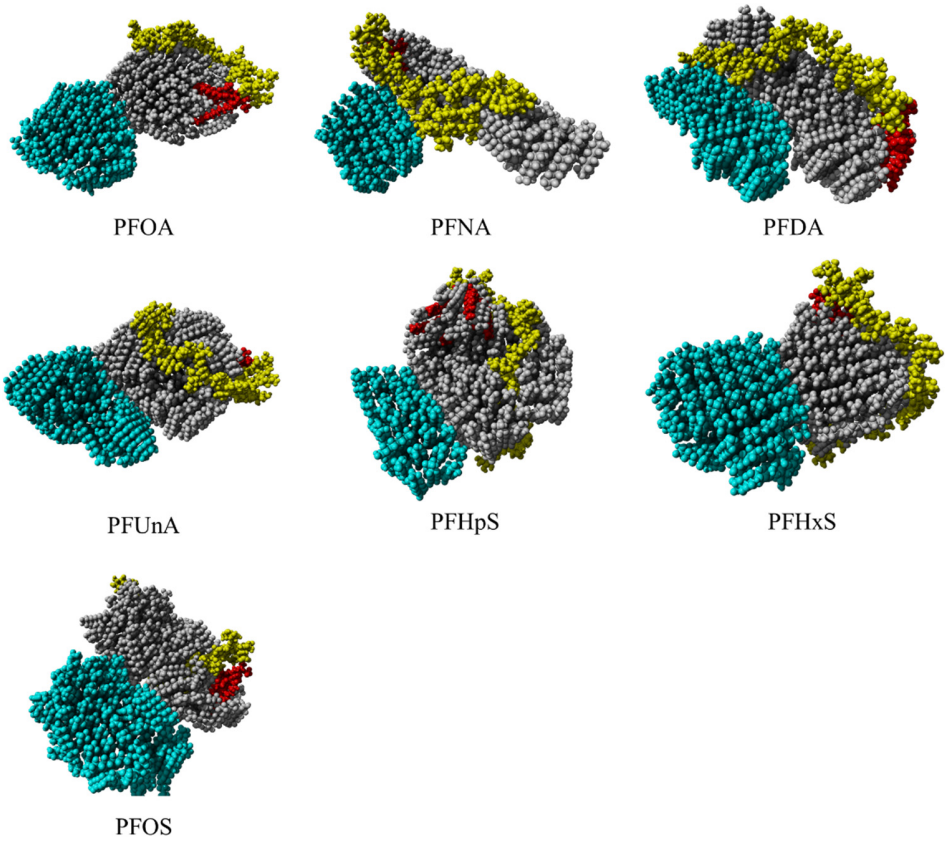

Fig. S15. Trajectories depicting the interaction between LPS and PFOA, PFNA, PFDA, PFUnA, PFHpS, PFHxS, and PFOS. LPS (polysaccharide, yellow; lipid A, red) and PFOS (complexed with LPS, gray; and self-aggregated, cyan).

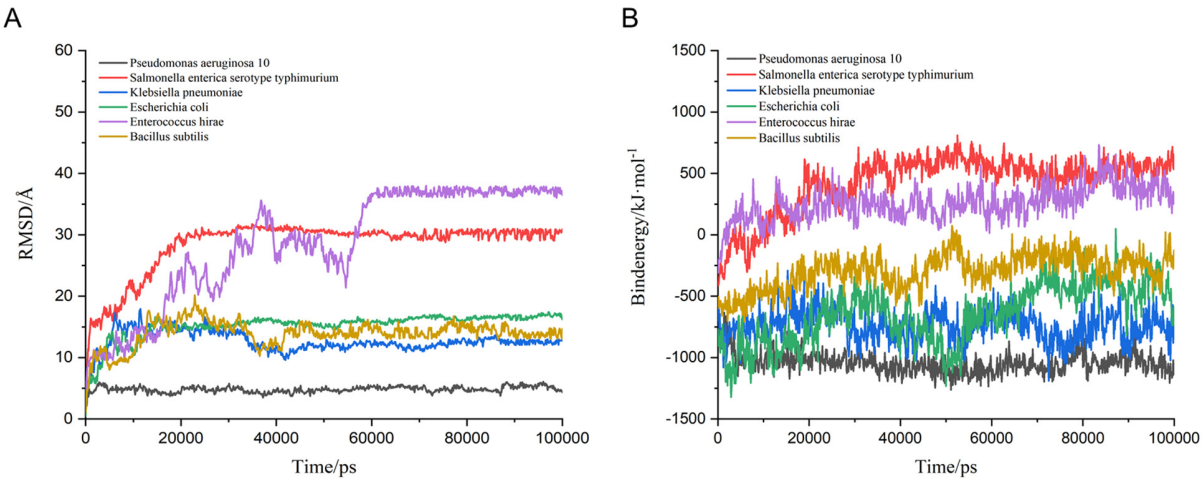

Fig. S16. Molecular dynamic simulations of LPS- or LTA-binding to PFOS. (*A*) Root-mean-squared deviation (RMSD) of the LPS- or LTA-PFOS (0–100 ns). (*B*) Binding energies (kJ/mol), LPS or LTA with PFOS (0–100 ns).

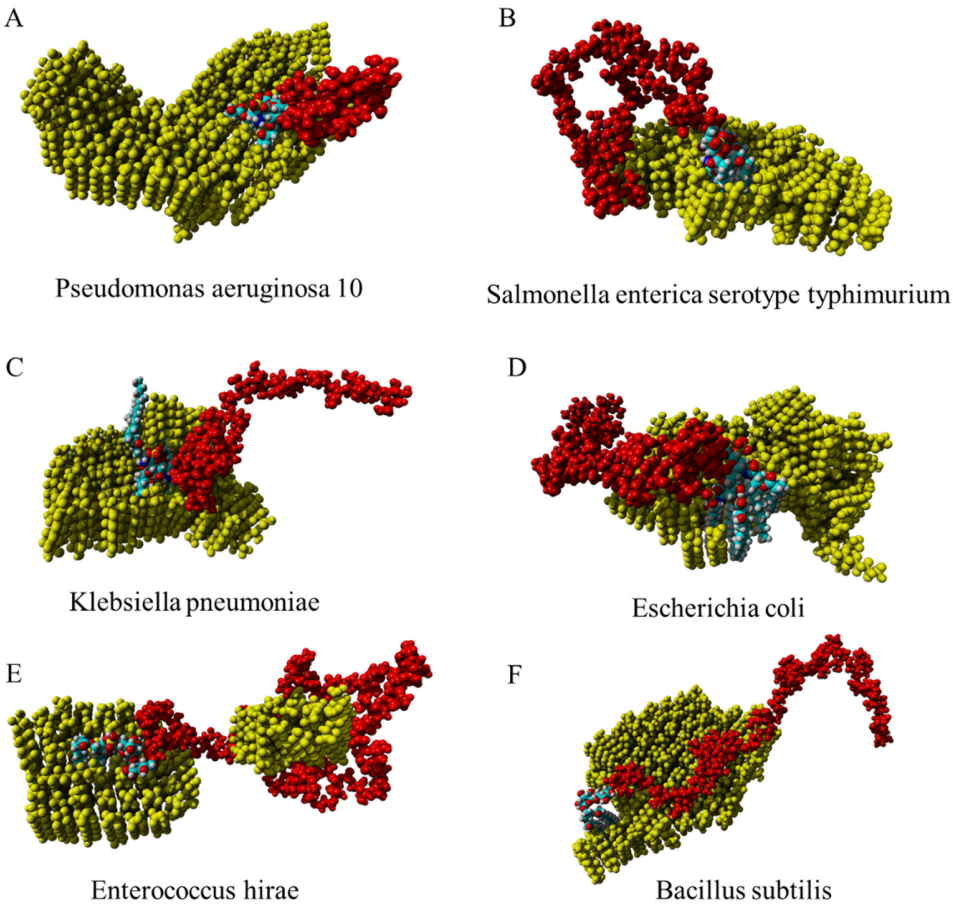

Fig. S17. Conformational changes of LPS derived from *P. aeruginosa 10* (*A*), *S. enterica serotype typhimurium* (*B*), *K. pneumoniae* (*C*), and *E. coli* (*D*); LTA derived from *E. hirae* (*E*) and *B. subtilis* (*F*) in the presence of PFOS. LPS and LTA (antigen, red; lipid, cyan) and PFOS (yellow).

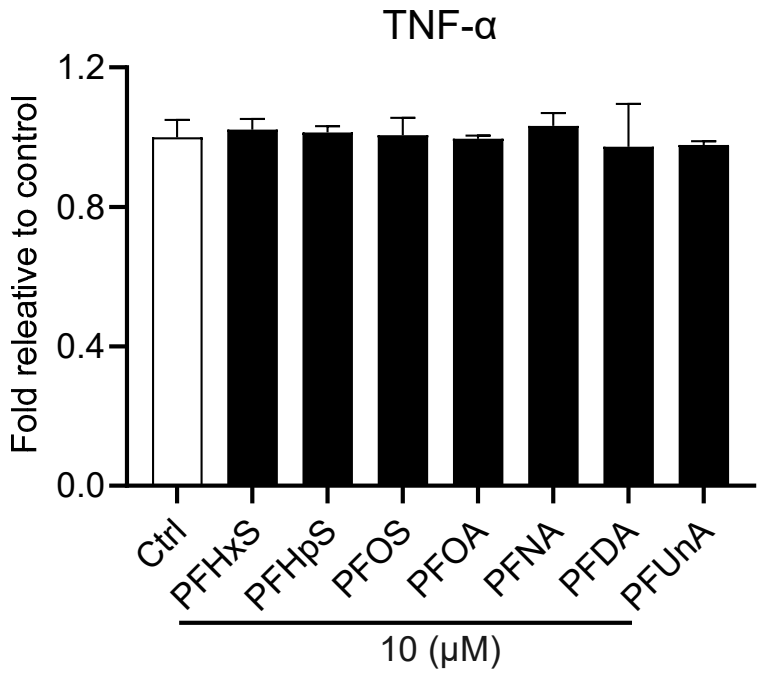

Fig. S18. PFCs at the highest dose (10 μM) without LPS did not affect the release of TNF-α from THP-1 macrophages. Values represent the mean and the standard error of the mean relative to the 0.1% DMSO vehicle control (n = 3).

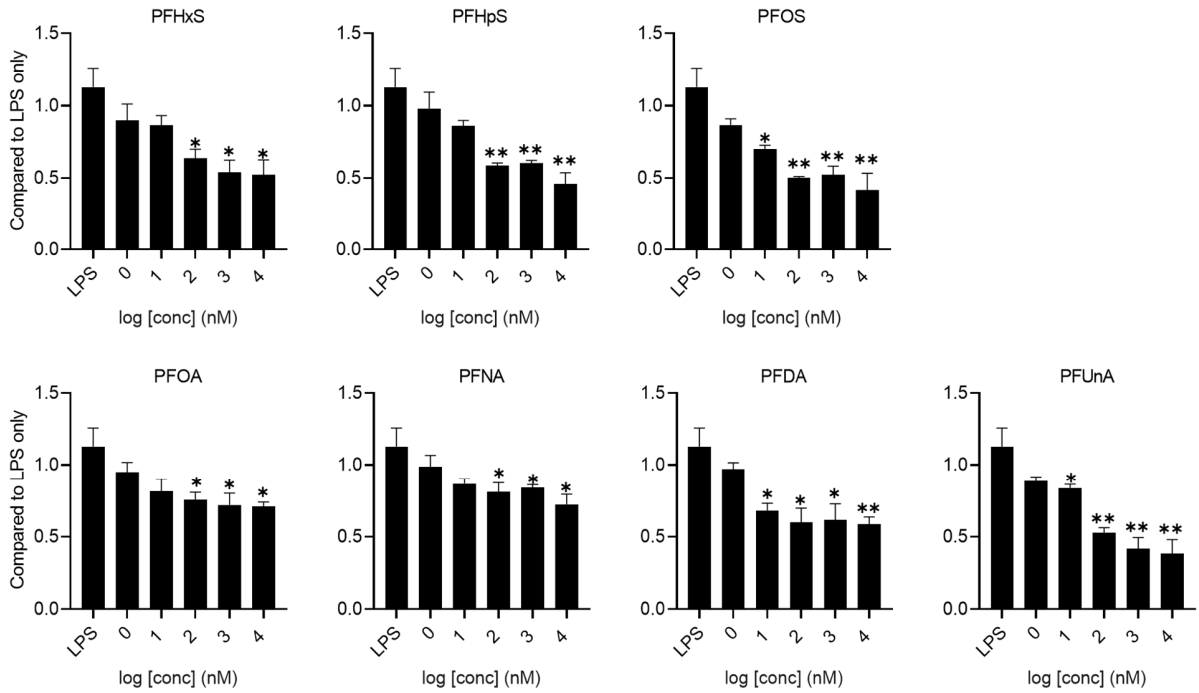

Fig. S19. Inhibition by PFCs of LPS-induced TNF-α production. Values represent mean and the standard error of the mean relative to the 0.1% DMSO vehicle control in the presence of *E. coli* LPS (n = 3). Significant differences vs the control simultaneously treated with *E. coli* LPS and PFCs: **p* < 0.05, ***p* < 0.01 (ANOVA).

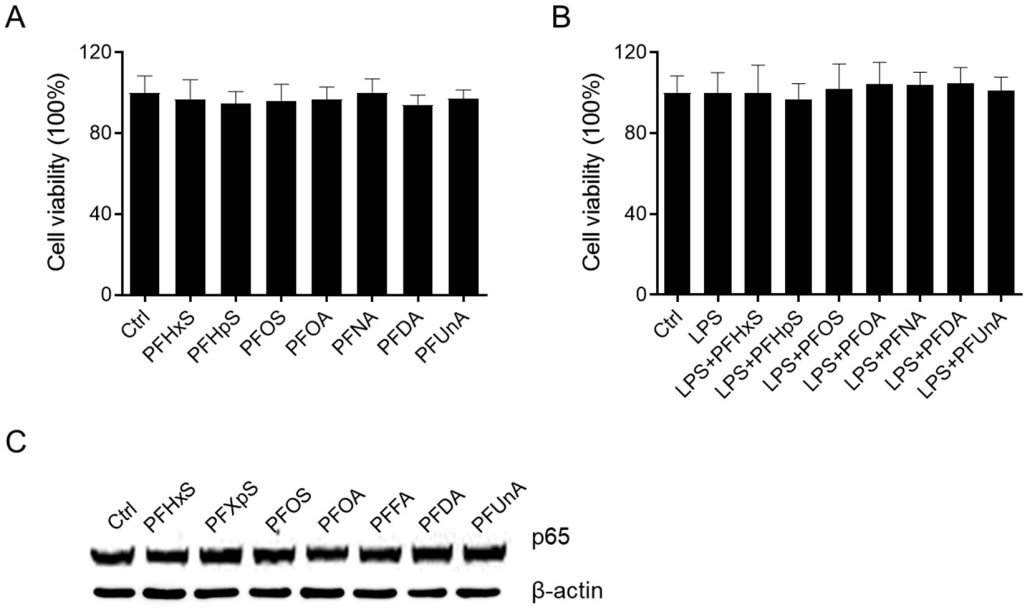

Fig. S20. (*A* and *B*) Viability of THP-1 macrophages exposed to PFCs (10 μM) (*A*), LPS (100 ng/mL) or LPS (100 ng/mL) + PFCs (10 μM) (*B*). Cells were analyzed after exposure 24 h. Values represent the mean and standard error of the mean (n = 3) vs the 0.1% DMSO control. (*C*) Western blot analysis of p65 phosphorylation in THP-1 macrophages treated with PFCs (100 nM).

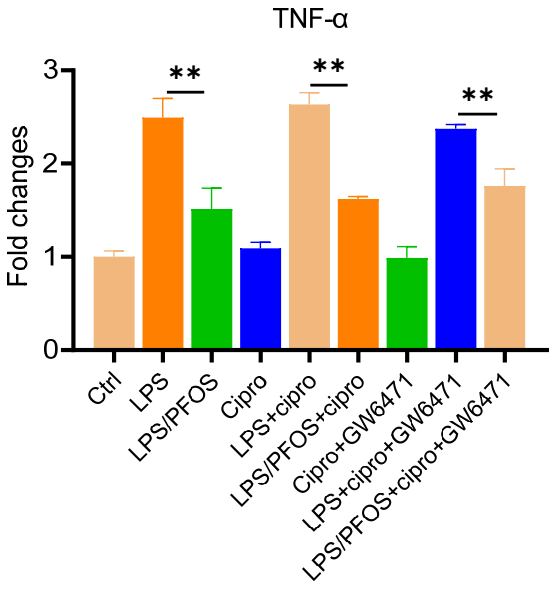

Fig. S21. Effects of the PPARα agonist ciprofibrate (20 μM) and antagonist GW6471 (5 μM) on cytokine production by THP-1 macrophages in the presence of either LPS alone or a mixture of 100 ng/mL LPS and 10 μM PFOS. Cipro = Ciprofibrate. Data are presented as the mean ± SEM of triplicates compared with the DMSO vehicle control. *$p < 0.05$, **$p < 0.01$ (ANOVA).

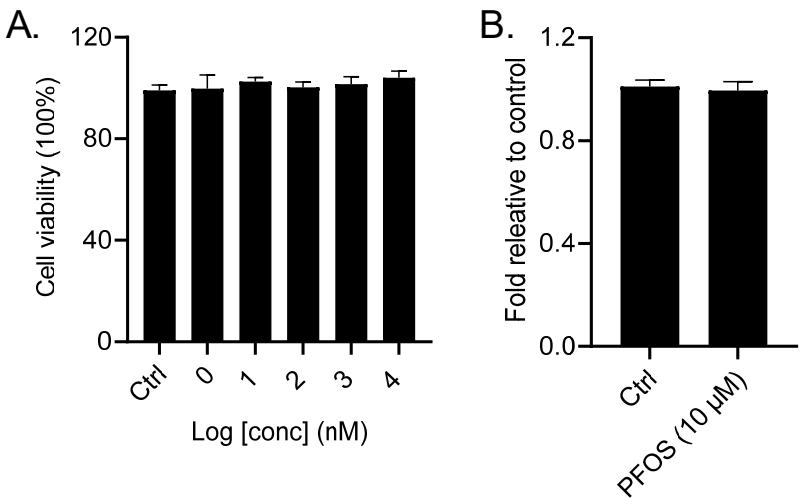

Fig. S22. (*A*) Viability of A549 cells exposed to PFOS. Cells were analyzed after exposure 24 h. (*B*) PFOS at the highest dose without LPS did not affect the release of TNF-α from A549 cells. Values represent the mean and the standard error of the mean relative to the 0.1% DMSO vehicle control (n = 3).

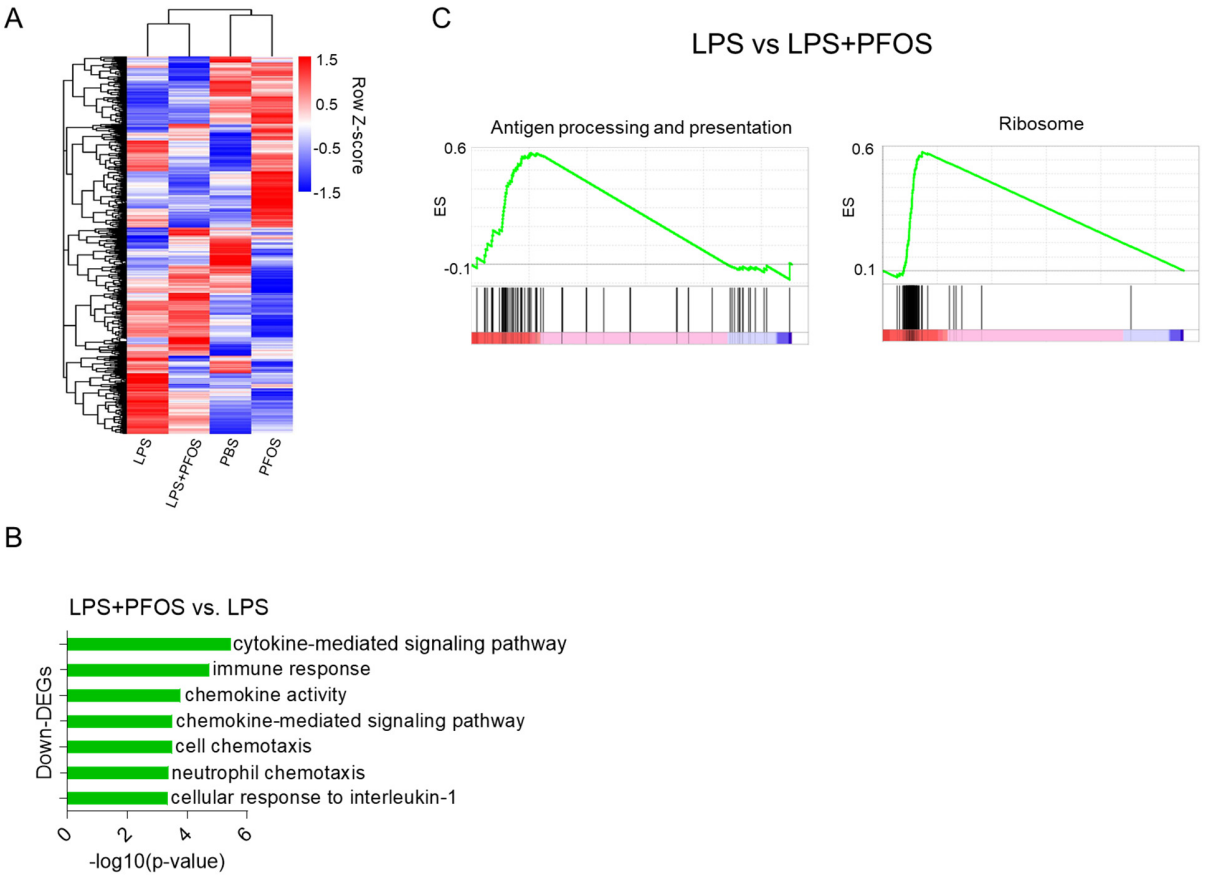

Fig. S23. Transcriptomic analysis of HENCs. (*A*) Hierarchical cluster analysis of common differentially expressed genes (DGEs) in the three treatment groups compared with the control group. (*B* and *C*) Gene Ontogeny (GO) enrichment (*B*) and gene set enrichment analysis (GSEA) (*C*).

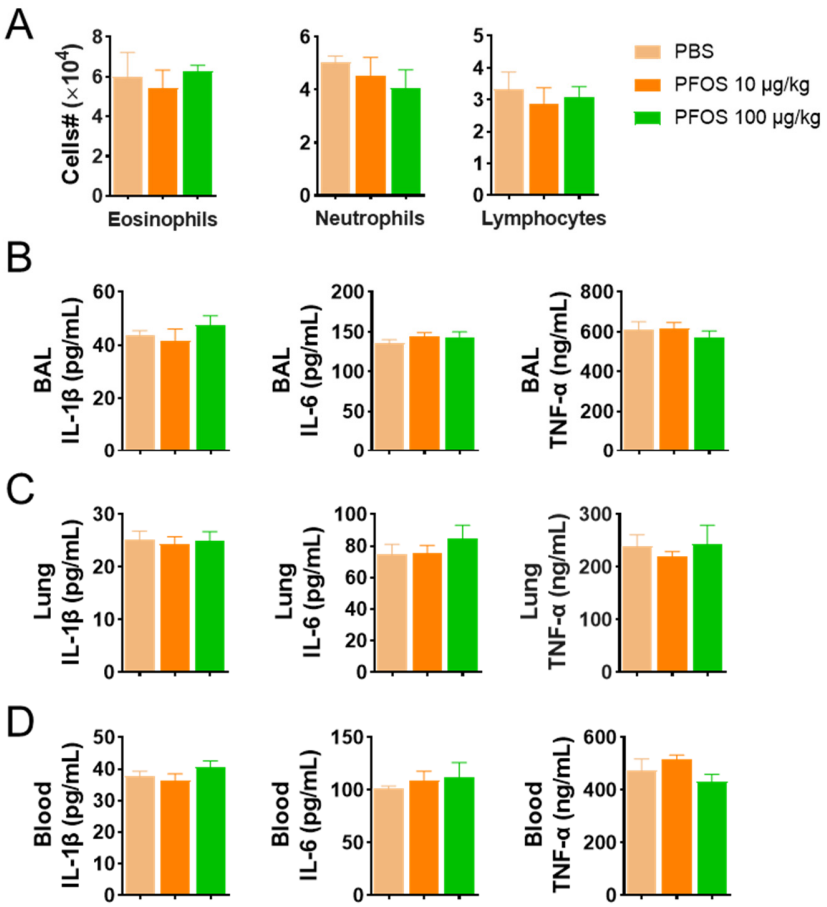

Fig. S24. Mice were pre-exposed to intranasal PFOS (10 μg/kg and 100 μg/kg) for 1 week, then intranasal with PBS without any introduction of bacteria. Mice were sacrificed 24 h after the infection. PFOS without *P. aeruginosa* did not affect (*A*) cell numbers in bronchoalveolar lavage (BAL) fluid. (*B-D*) proinflammatory cytokines, including IL-1β, IL-6, TNF-α from the BAL (*B*), lung (*C*), and blood (*D*). Data represent the mean ± SEM (n = 5 mice per group).

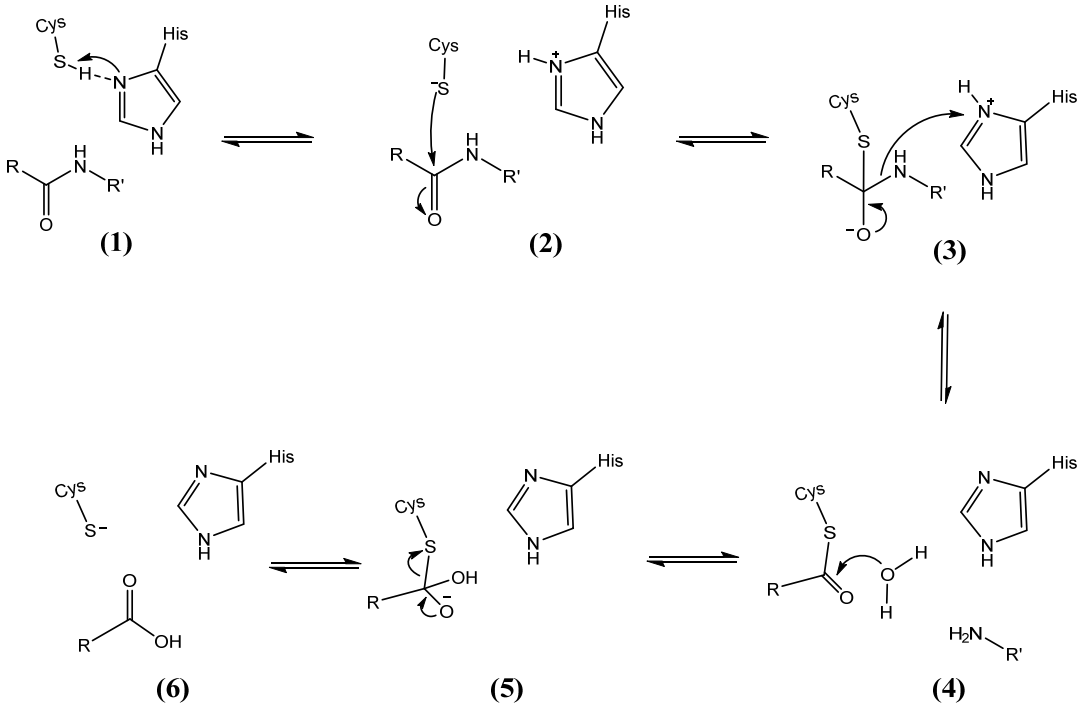

Fig. S25. General mechanism of Der p1 catalysis.

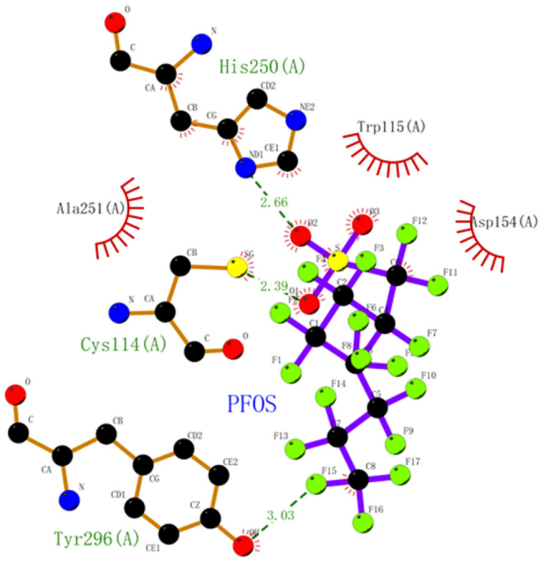

Fig. S26. Molecular docking of PFOS with Der p1 (PDB, 1XKG). 2D: PFOS is purple, hydrophobic residues are depicted as radial arcs, and hydrogen bonds are indicated by the dotted green lines.

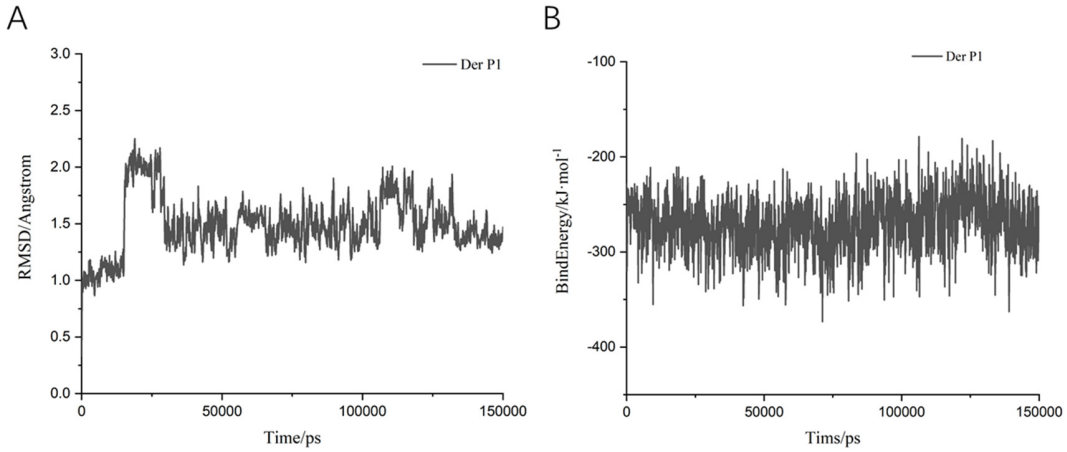

Fig. S27. Molecular dynamic simulations of Der p1 binding to PFOS. (*A*) Root-mean-squared deviation (RMSD) of Der p1-PFOS (0–100 ns). (*B*) Binding energies (kJ/mol), der p1 with PFOS (0–100 ns).

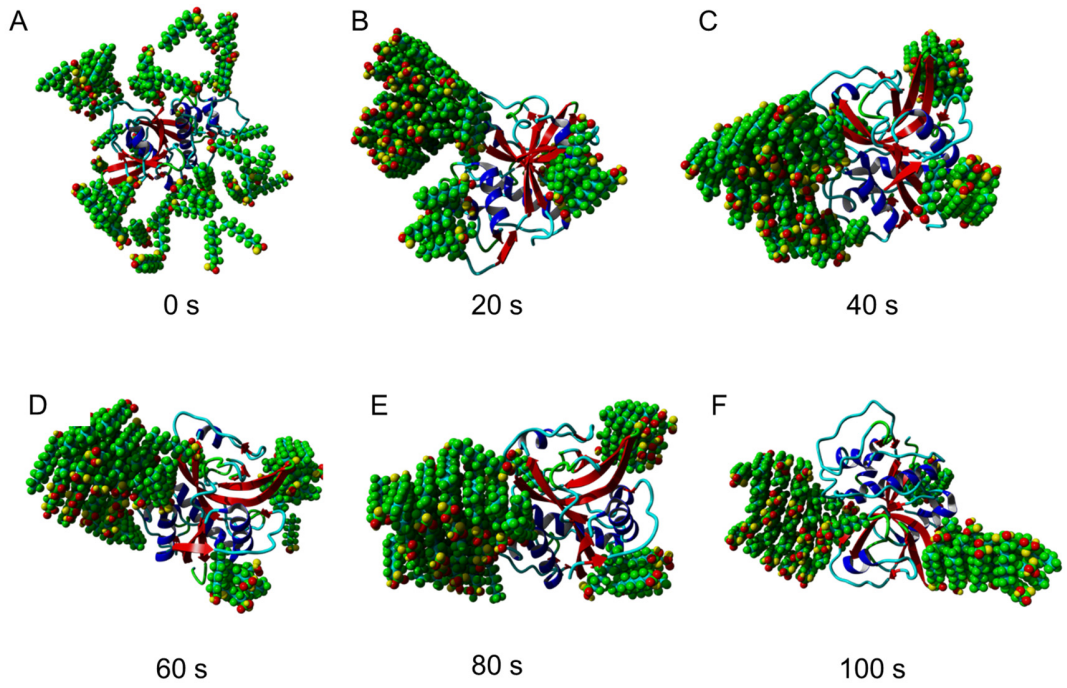

Fig. S28. Trajectories depicting PFOS gathering around Der p1 for 0, 20, 40, 60, 80, and 100 ns. PFOS, green; protein, elastic band.

Table S1. The primer sequences of target mRNA genes.

Gene names	Primers sequence (5'-3')	Accession numbers
Mus musculus interleukin 5 (Il5)	F: 5' ATGAAGTGCTGGAGATGG 3' R: 5' GGATGCTAAGGTTGGGTATG 3'	NM_010558.1
Mus musculus interleukin 10 (Il10)	F: 5' AGGACTTTAAGGGTTACTTG 3' R: 5' CAAATGCTCCTTGATTTCTG 3'	NM_010548.2
Mus musculus interleukin 13 (Il13)	F: 5' ATTGCATGGCCTCTGTAACC 3' R: 5' GGCGAAACAGTTGCTTTGTG 3'	NM_008355.3
Mus musculus interleukin 17 receptor B (Il17)	F: 5' CCTGGTGGTTTATCCTTCTG 3' R: 5' TTATCTGCCGCTTGCTTC 3'	NM_019583.3
Mus musculus interferon gamma (Ifnγ)	F: 5' TCAAGTGGCATAGATGTG 3' R: 5' TGTTGCTGAAGAAGGTAG 3'	NM_008337.4
Mus musculus mucin 5, subtypes A and C, tracheobronchial/gastric (Muc5ac)	F: 5' GTCTCCCTGGATGGATGTTAG 3' R: 5' ACTTGGCAGATTGGGTAGC 3'	NM_010844.3
Mus musculus tumor necrosis factor, alpha-induced protein 3 (Tnfaip3)	F: 5' AGTATCCCTGCCTCCTGTC 3' R: 5' TGCTTGTCCCTGCTCTGTC 3'	NM_001166402.1
Mus musculus glyceraldehyde-3-phosphate dehydrogenase (Gapdh)	F: 5' ATCACTGCCACCCAGAAG 3' R: 5' TCCACGACGGACACATTG 3'	NM_008084.2

Table S2. Literature values of the geometric mean and maximum of serum PFC concentrations (nM) in children.

Chemical	Median (nmol)	Max (nmol)
PFHxS	2.39	22.74
PFOS	43.52	207.41
PFOA	5.46	33.33
PFNA	1.48	6.77
PFDA	0.95	5.69
PFHpS	0.63	3.52
PFUnA	0.39	3.38

Table S3. LPS inactivation by PFCs.

Chemical	LOEL (nM)	LI Max[a]	EC_{20} (nM)	EC_{30} (nM)
PFHxS	< 1.0	0.31	< 1.0	1137
PFHpS	< 1.0	0.34	< 1.0	110
PFOS	< 1.0	0.57	< 1.0	35
PFOA	< 1.0	0.26	562	> 10000
PFNA	< 1.0	0.29	1.42	> 10000
PFDA	< 1.0	0.36	< 1.0	504
PFUnA	< 1.0	0.43	< 1.0	422

LOEL = lowest observed effect level, the lowest concentration (nM) that exhibited significant activity vs the DMSO vehicle control. [a]LPS inactivation (LI) (relative to vehicle control) shown as maximum efficacies. EC_{20} and EC_{30} values (nM) (concentrations required to reduce effect by 20% and 30%, respectively).

Table S4. Bioactivity inactivation potencies ($EC_{20/30}$) and efficacies (Max) of PFOS-treated LPS preparations from *S. Typhimurium*, *P. aeruginosa* 10, *K. pneumoniae*, and *P. vulgaris* and LTA from *B. subtilis* and *E. hirae*.

Bacterial Strains	LOEL (nM)	LI Max[a]	EC_{20} (nM)	EC_{30} (nM)
S. Typhimurium LPS	10	0.32	1.31	> 10000
P. aeruginosa 10 LPS	1.0	0.42	< 1.0	< 1.0
E. hirae LTA	10	0.44	< 1.0	9.2
B. subtilis LTA	1.0	0.37	< 1.0	1.24
P. vulgaris LPS	10000	0.30	2.06	> 10000
K. pneumoniae LPS	10	0.45	< 1.0	1.29
Gut microbiome LPS	1.0	0.43	< 1.0	1.41

LOEL = lowest observed effect level, the lowest concentration (nM) that exhibited significant activity vs the DMSO vehicle control. [a]LPS inactivation (LI) (relative to vehicle control) shown as maximum efficacies. EC_{20} and EC_{30} values (nM) (concentrations required to reduce effect by 20% and 30%, respectively).

SI References

1. A. M. Calafat, L. Y. Wong, Z. Kuklenyik, J. A. Reidy, L. L. Needham, Polyfluoroalkyl chemicals in the US population: data from the National Health and Nutrition Examination Survey (NHANES) 2003–2004 and comparisons with NHANES 1999–2000. *Environ. Health. Perspect.* **115**, 1596-1602 (2007).
2. G. H. Dong, K. Y. Tung, C. H. Tsai, M. M. Liu, D. Wang, W. Liu, Y. H. Jin, W. S. Hsieh, Y. L. Lee, P. C. Chen, Serum polyfluoroalkyl concentrations, asthma outcomes, and immunological markers in a case–control study of Taiwanese children. *Environ. Health. Perspect.* **121**, 507-513 (2013).
3. S. Jo, T. Kim, V. G. Iyer, W. Im, CHARMM-GUI: a web-based graphical user interface for CHARMM. *J. Comput. Chem.* **29**, 1859-1865 (2008).
4. J. Lee, X. Cheng, J. M. Swails, M. S. Yeom, P. K. Eastman, J. A. Lemkul, S. Wei, J. Buckner, J. C. Jeong, Y. Qi, CHARMM-GUI input generator for NAMD, GROMACS, AMBER, OpenMM, and CHARMM/OpenMM simulations using the CHARMM36 additive force field. *J. Chem. Theory Comput.* **12**, 405-413 (2015).
5. H. J. C. Berendsen, D. Vanderspoel, R. Vandrunen, Gromacs-a Message-Passing Parallel Molecular-Dynamics Implementation. *Comput. Phys. Commun.* **91**, 43-56 (1995).
6. U. Essmann, L. Perera, M. L. Berkowitz, T. Darden, H. Lee, L. G. Pedersen, A smooth particle mesh Ewald method. *J. Chem. Phys.* **103**, 8577-8593 (1995).
7. C. W. Yap, PaDEL-descriptor: an open source software to calculate molecular descriptors and fingerprints. *J. Comput. Chem.* **32**, 1466-1474 (2011).
8. G. M. Morris, R. Huey, W. Lindstrom, M. F. Sanner, R. K. Belew, D. S. Goodsell, A. J. Olson, AutoDock4 and AutoDockTools4: Automated docking with selective receptor flexibility. *J. Comput. Chem.* **30**, 2785-2791 (2009).
9. J. Fuhrmann, A. Rurainski, H. P. Lenhof, D. Neumann, A new Lamarckian genetic algorithm for flexible ligand-receptor docking. *J. Comput. Chem.* **31**, 1911-1918 (2010).
10. H. Y. Sun, F. Q. Ji, L. Y. Fu, Z. Y. Wang, H. Y. Zhang, Structural and energetic analyses of SNPs in drug targets and implications for drug therapy. *J. Chem. Inf. Model.* **53**, 3343-3351 (2013).
11. H. Y. Sun, T. J. Hou, H. Y. Zhang, Finding chemical drugs for genetic diseases. *Drug Discov. Today* **19**, 1836-1840 (2014).
12. M. F. Sanner, Python: a programming language for software integration and development. *J. Mol. Graph. Model.* **17**, 57-61 (1999).
13. C. Ultra, 12.0, Cambridge Soft, Cambridge, MA 2010. *May*, (2013).
14. A. Pedretti, L. Villa, G. Vistoli, VEGA: a versatile program to convert, handle and visualize molecular structure on Windows-based PCs. *J. Mol. Graph. Model.* **21**, 47-49 (2002).
15. M. D. Hanwell, D. E. Curtis, D. C. Lonie, T. Vandermeersch, E. Zurek, G. R. Hutchison, Avogadro: an advanced semantic chemical editor, visualization, and analysis platform. *J. Cheminformatics* **4**, 1-17 (2012).
16. H. J. Berendsen, D. van der Spoel, R. van Drunen, GROMACS: a message-passing parallel molecular dynamics implementation. *Comput. Phys. Commun.* **91**, 43-56 (1995).
17. T. Polte, J. Foell, C. Werner, H. G. Hoymann, A. Braun, S. Burdach, R. S. Mittler, G. Hansen, CD137-mediated immunotherapy for allergic asthma. *J. Clin. Invest.* **116**, 1025-1036 (2006).
18. V. Sharma, B. P. Singh, N. Arora, Cur l 3, a Major Allergen of Curvularia lunata–Derived Short Synthetic Peptides, Shows Promise for Successful Immunotherapy. *Am. J. Respir. Cell Mol. Biol.* **45**, 1178-1184 (2011).
19. P. Langfelder, S. Horvath, WGCNA: an R package for weighted correlation network analysis. *BMC Bioinform.* **9**, 559 (2008).
20. E. Corsini, E. Sangiovanni, A. Avogadro, V. Galbiati, B. Viviani, M. Marinovich, C. L. Galli, M. Dell'Agli, D. R. Germolec, In vitro characterization of the immunotoxic potential of several perfluorinated compounds (PFCs). *Toxicol. Appl. Pharmacol.* **258**, 248-255 (2012).
21. J. Sambrook, D. Russell, *Molecular cloning: a laboratory manual., 3rd edn.(Cold Spring Harbor Laboratory Press: New York)* (2001).